Chapter 6 Zinc-air Batteries using $MoSe_2$ based Nanomaterials as Air cathode

6.1 Introduction

To meet the energy demand, it is imperative to advance the development of high-energy storage systems to utilize energy generated by renewable sources during their high demands [175]. Lead-acid batteries were popular for electric vehicle propulsion in the 1990s, but their low energy density limited their usage. Currently, most electric vehicles, especially cars, are adopting lithium-ion batteries for propulsion. Lithium-ion batteries can only cover a distance of 160 kilometres per charge, which contributes to a substantial part (65%) of their cost. This is primarily due to their lower energy density in comparison to gasoline. Gasoline has an energy density of 13,000 Wh kg^{-1}, whereas lithium-ion batteries have an energy density ranging from 200 to 500 Wh kg^{-1} [14, 176, 177]. The Pb-acid, Ni-Cd, and Li-ion batteries are prevalent in portable electronics and electric vehicles. Li-ion batteries have a higher energy density relative to their physical size, a low self-discharge rate of 1.5 percent per month, and zero to low memory effect. It can typically manage hundreds of chare-discharge cycles, while mid-grade variants can handle 1000 cycles before losing 30 percent of their original maximum charge capacity. Unlike other batteries, Li-ion batteries require very little, if any, maintenance. Although Li-ion battery possesses several advancements, still it remains insufficient for enhancing the range of electric vehicle propulsion due to their high production cost, environmental hazards, aging effect, deep discharge, short circuit by overcharge, over discharge, and low practical energy density.

To perform long run, electric vehicles must have great specific energy and power density. The attainment of a long driving range is positively correlated with a high specific energy density,

whereas the ability for rapid acceleration and hill-climbing is proportional to the presence of a high specific power density [178]. Due to their open battery design, utilizing air as a reagent, metal-air batteries (MABs) have significantly higher specific capacities [179, 180]. However, MABs face significant challenges that must be resolved before being utilized in applications. MABs with open-cell structure allow ambient oxygen to flow into cathode material, which differs from closed/packed lithium-ion batteries. They are composed of air cathode, metal anode, electrolyte, and a separator as shown in **Figure 6.1 (a)**. Various electrocatalysts such as porous carbon materials and metals like Na, Fe, Li, Mg, K and Zn have been extensively investigated for use in air cathodes and metal anodes, respectively [181]. Redox (reduction/oxidation) reaction takes place during the battery operation. The metal anode dissolves in the electrolyte, whereas oxygen reduction reaction (ORR) and oxygen evolution reaction (OER) take place at air cathode during discharging and charging of the MABs, respectively [182]. The theoretical energy density of various MABs, such as Mg-air, Li-air, Na-air, K-air, and zinc-air batteries, are illustrated in **Figure 6.1** (b). Among the shown MABs, zinc-air batteries have several advantages like they are electrically rechargeable, safe, environmentally friendly, cost-effective, and easy to store and deliver electrical energy for both portable and stationary devices. Zinc is inexpensive and abundant in nature in the earth's crust as compared to Li minerals [183].

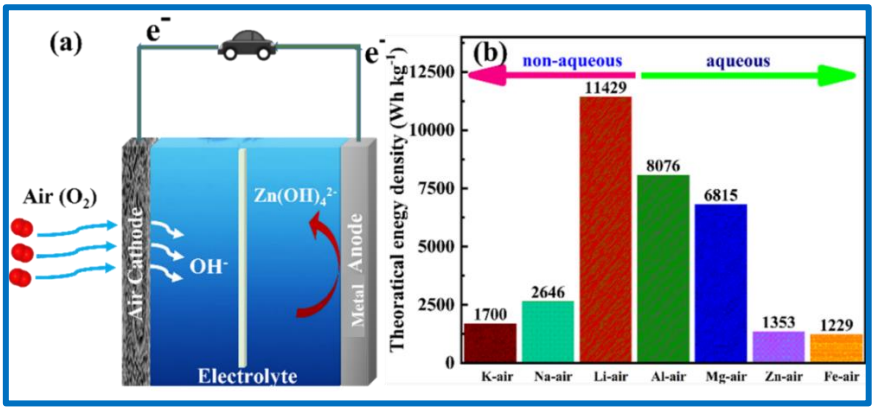

Figure 6.1 *(a) Schematic diagram of a typical metal-air battery and (b) theoretically estimated energy densities of various types of metal-air batteries* [180].

The zinc-air batteries can be considered as fuel cells as well as batteries [184, 185]. In zinc-air batteries, the Zn metal acts as fuel and catalytic reaction can be controlled by varying the controlled flow of air. Prior studies elucidate that zinc and iron in metallic form are more stable or robust, have higher cell voltage and higher energy in a liquid or aqueous electrolyte and can be charged more efficiently in aqueous electrolytes [186]. Electrochemical reactions involved during the battery discharge are discussed below-

Discharge:

At anode: $$Zn \rightarrow Zn^{2+} + 2e^{-} \quad (6.1)$$

Electrons are liberated at Zn anode during oxidation **reaction 6.1**

$$Zn + 4OH^{-} \rightarrow Zn(OH)_4^{2-} + 2e^{-} \quad (6.2)$$

During the discharge process, metallic Zn anode in contact with the alkaline electrolyte generates zincate ion (**reaction 6.2**).

$$Zn(OH)_4^{2-} \rightarrow ZnO + H_2O + 2OH^{-} \quad (6.3)$$

Generated zincate ion decomposed to form solid ZnO powder (**reaction 6.3**).

Cathode: $$O_2 + 2H_2O + 4e^{-} \rightarrow 4OH^{-} \quad (6.4)$$

$$O_2 + H_2O + 2e^{-} \rightarrow HO_2^{-} \quad (6.5)$$

$$HO_2^{-} + H_2O + 2e^{-} \rightarrow 4OH^{-} \quad (6.6)$$

$$HO_2^{-} \rightarrow 2OH^{-} + O_2 \quad (6.7)$$

There are two types of pathways $4e^{-}$ (**reaction 6.4**) or $2e^{-}$ (**reaction 6.5, 6.6**) occurs at the metal catalyst surface embedded in air cathode during ORR in aqueous electrolyte media as described in reactions. The $4e^{-}$ pathway is the direct reaction and it is more favorable than the $2e^{-}$ pathway because of its enhanced energy efficiency. The $2e^{-}$ reaction pathway unfavorably

affects the formation of peroxide species, which causes corrosiveness and leads to untimely degradation of the zinc-air battery. Simultaneously, diffused oxygen molecules into porous air electrodes are reduced into hydroxyl ions (OH^-) in ORR (**reaction 6.4**), which migrate from one end cathode to another end anode. There are other possibilities as well which follows the $2e^-$ reaction pathway: reduction of peroxide (**reaction 6.5**) and chemical disproportionation of peroxide (**reactions 6.6 and 6.7**). The overall reaction is mentioned in **reaction 6.8**.

Overall reaction: $$2Zn + O_2 \rightarrow 2ZnO \quad (6.8)$$

Parasitic reaction:

$$Zn + 2H_2O \rightarrow Zn(OH)_2 + H_2 \uparrow \quad (6.9)$$

The parasitic reaction liberates hydrogen gas, which dampens the battery's performance during the discharge (**reaction 6.9**). Reactions involved during the battery recharge are discussed below-

Recharge:

Anode:

$$ZnO + H_2O + 2OH^- \rightarrow Zn(OH)_4^{2-} \quad (6.10)$$

$$Zn(OH)_4^{2-} + 2e^- \rightarrow Zn + 4OH^{-\,2-} \quad (6.11)$$

During recharge, at the anode, this reaction (**reactions 6.10,6.11**) pathways are reversed of discharge during the recharge to reduce zincate ions back to zinc.

Cathode:

$$4OH^- \rightarrow O_2 + 2H_2O + 4e^- \quad (6.12)$$

At the same time cathode releases oxygen which nothing but OER (**reaction 6.12**) [175].

Overall reaction:

$$2ZnO \rightarrow 2Zn + O_2 \quad (6.13)$$

If we say precisely, during recharge discharge, ZnO powder is converted back into oxygen and metallic zinc (**reaction 6.13**).

6.1.1 Battery performance analysis

There are some following key parameters which evaluate the performance of rechargeable zinc-air batteries.

6.1.1.1 Open circuit potential (OCP)

Open circuit potential (OCP) measurements play a crucial role in studying and operating zinc-air batteries. The OCP is the potential difference or voltage across the battery terminals when no current is drawn. It is also called the rest mode of the battery. It represents the maximum potential difference the battery can provide. In the context of zinc-air batteries, OCP measurements can provide valuable insights into the battery's state of charge and overall health.

6.1.1.2 Galvanostatic full-discharge

The galvanostatic full-discharge test is a technique used to measure the specific capacity (C_d) of a zinc-air battery. This can be done by applying a constant discharge current density ($mA.cm^{-2}$) until a specific cut-off voltage is achieved. The mass of zinc electrode determines the capacity of a zinc-air battery. Therefore, it is common to normalize the capacity by the mass of the zinc electrode or the amount of utilized zinc after discharge of the battery. It is calculated using the following **equation 6.14**

$$C_d = I_d \times \Delta T_d / m_{Zn} \qquad (6.14)$$

Where I_d denotes the discharge current (mA), ΔT signifies the discharge time (h), and m_{Zn} represents the consumed mass of zinc metal (g). Typically, the actual specific capacity density is less than its theoretical counterpart due to unavoidable side reactions occurring at the zinc anode, which will be discussed in subsequent sections. The specific energy density (E_d) represents the amount of energy that can be stored in a given volume or mass of the battery. It

is typically expressed in watt-hours per litre (WhL^{-1}) or watt-hours per kilogram ($Whkg^{-1}$), which could be estimated by the following **equation 6.15**-

$$E_d = C_d \times V_d \quad (6.15)$$

Where C_d describes the discharge-specific capacity measured in milliampere-hours per gram of Zinc (mA h g_{Zn}^{-1}), while V_d stands for the discharge working potential, measured in volts (V). The comparison of the discharge performance of the catalyst on a zinc-air battery is restricted by the specific energy density, which is calculated based on the consumption of metallic zinc.

6.1.1.3 Galvanodynamic discharge polarization

The galvanodynamic discharge polarization technique is used to assess a battery's power density. It measures the deviation of the operating voltage of a battery from its OCP when discharging and charging currents are applied. This is done by applying negative discharging currents of increasing magnitude to the battery electrodes and recording the potential responses as a function of the current. The difference between the operating voltage and the OCP, known as the discharge overpotential, represents the total voltage losses associated with activation and mass-transfer polarization at the electrode and the ohmic resistance of every component of the electrochemical circuit. The power density (P_d) is the measure of energy output ($mWcm^{-2}$) to deliver per hour, calculated by multiplying the discharge current density and the voltage derived from the polarization curves (**equation 6.16**).

$$P_d = I_d \times V_d \quad (6.16)$$

Where I_d and V_d discharge current density and voltage, respectively.

6.1.1.4 Galvanostatic cycling

Galvanostatic cycling is a method employed to assess the electrochemical longevity of zinc-air batteries. This technique involves alternating fixed negative and positive currents while

monitoring the corresponding discharge and charge voltages. Unlike galvanodynamic polarization testing, galvanostatic cycling offers a wider range of test conditions, including discharge/charge current density, the cycle count, and the duration or cut-off voltage for each cycle. Cycling involves a large number of cycles with brief durations for each cycle, known as pulse cycling. In this approach, the cycling durability is likely constrained by the air electrode, as the zinc electrode is typically discharged to only a small percentage of its total capacity in each cycle. Cycle life refers to the number of charge-discharge cycles a battery can undergo before its capacity significantly decreases. It is an essential metric for rechargeable batteries, indicating their longevity and durability.

6.1.1.5 Role of electrocatalyst in rechargeable zinc-air batteries

Zinc-air batteries seem to be a technically and economically feasible solution for the fast-charging of electrical and electronic devices in future [61, 183, 187, 188]. In rechargeable zinc-air batteries, catalyst material at the cathode is critically responsible for performance. To develop feasible zinc-air battery systems, novel, efficient, inexpensive, and durable catalysts are required. Transition metals (such as Co, Ni, Fe, and Cu), their oxides, phosphates, sulfates, dichalcogenides, first-row transition metal spinels, perovskites, carbon nanostructures and metalorganic frameworks are expected as potential catalysts for batteries [189-194]. Metal oxides such as Co_3O_4, MnO_2, $NiCo_2O_4$ and others are promising materials for zinc-air batteries due to their high electrocatalytic activity, low cost, non-toxicity, abundance and stability in variety of environments, including high temperatures and harsh chemicals [39-44]. However, these materials suffer from low conductivity and poor oxygen mobility, which can limit their performance. TMDs can be considered to be good electrocatalysts due to their fascinating properties like good conductivity and high surface area, which can show the enhanced activity by site doping, control of growth morphology, and heterostructure formation.

In the recent past, there have been few studies on carbon and MoS_2 based air cathodes for zinc-air battery. Liu *et al.* developed a facile strategy to directly grow cobalt nanoparticles embedded in N-doped carbon nanotube arrays (Co@NCNTAs) on carbon cloth substrates and showed high specific capacity of 368 mAh g^{-1} for flexible solid-state zinc-air battery at a current density of 2 mA cm^{-2} and power density of 38.6 mW cm^{-2} [69] Wang *et al*. reported a tri-doped graphene with N, S, and P for better electrocatalytic oxygen reactions. The tri-doped graphene, as a cathode catalyst, provides a power density up to 225 mW cm^{-2} as well as good long-term charge-discharge durability for rechargeable zinc-air battery [70]. Challa *et al*. demonstrated MoS_2/graphene hybrid nanoplatelets as zinc-air battery cathode using bovine serum albumin (BSA) as an exfoliant for MoS_2 sheets to synthesize hybrid sample. They demonstrated flexible, and bioabsorbable/biodegradable zinc-air battery with high open-circuit voltage of 1.4 V and energy density of 130 W h kg^{-1} [71] As a durable electrocatalyst, MoS_2@FeN-C nanosphere interfaced with single Fe atoms was investigated for wearable zinc-air battery, which exhibits remarkable deformation stability, high specific capacity (442 mA h $g^{-1}{}_{Zn}$) and excellent power density (78 mW cm^{-2}) [72]. The zinc-air battery with heterolayered MoS_2/Graphene nanosheets shows specific energy density of 130 W h kg^{-1}, while $Co(Zn_{0.5})$@MoS_2/CC based zinc-air battery exhibits power density of 72.4 mW cm^{-2} [65]. Ling *et al.* demonstrated Co_3O_4/WS_2 based zinc-air battery showing the specific capacity of 830 mAh $g^{-1}{}_{Zn}$ and overpotential (η_{10}~ 330 mV) [67]. In spite of these efforts, the real potential of zinc-air batteries is yet to be explored so that theoretically expected energy density can be achieved. $MoSe_2$ can also be a good electrocatalyst due to its low-cost synthesis, low onset potential, high electrochemical activity, and long-term stability [68]. In the following section, we will discuss the performance of the zinc-air batteries using $MoSe_2$, and its, hybrid nanostructures with bimetal oxides ($NiCo_2O_4$/NiO-$MoSe_2$, $CoFe_2O_4$-$MoSe_2$ and $NiFe_2O_4$-$MoSe_2$) as air cathodes.

6.2 Results and discussion

In the present work, we have successfully synthesized $MoSe_2$, $CoFe_2O_4$, $NiCo_2O_4$/NiO, $NiFe_2O_4$, and hybrid nanostructures ($CoFe_2O_4$-$MoSe_2$, $NiCo_2O_4$/NiO-$MoSe_2$, and $NiFe_2O_4$-$MoSe_2$) and utilized these nanostructures as air cathode in zinc-air batteries.

6.2.1 Assembly of zinc-air battery

An electrochemical device has been fabricated using prepared materials coated carbon cloth as a cathode and a zinc metal sheet (thickness: 200 µm) as anode for energy storage in zinc-air battery system. Both electrodes are taken of 1 cm^2 dimensions and fixed on either side of the electrolytic chamber. The electrolytic chamber is filled with alkaline electrolyte (6M KOH + 0.2 M $Zn(CH_3CO_2)_2.2H_2O$).

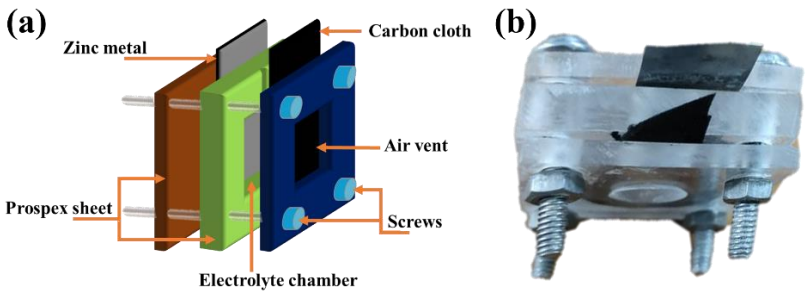

Figure 6.2 *(a) Schematic of a typical zinc-air battery and (b) photograph of fabricated zinc-air battery.*

Figure 6.2 represents the schematic (Figure 6.2a) and indigenously design of zinc-air battery device (Figure 6.2b), which is fabricated using an acrylic sheet. The battery cell is a prototype with a total cell capacity of 2 mL for electrolyte. It has two replaceable electrode support structures which serve as a support to the cathode and anode. The cell has been equipped with connections to both prepared materials-based cathode and zinc anode. The electrode's power connection terminals are freely accessible from the outside. The electrode replacement is made exceedingly simple by the design of the device. The OCP, specific

capacity, energy density, and power density of designed batteries have been calculated to understand their performance.

6.2.2 Zinc-air battery performance using pristine $MoSe_2$ as air cathode

Hydrothermally produced $MoSe_2$ nanosheets show good catalytic activity for OER as discussed in chapter 4, that prompted us to use it as an air cathode in zinc-air battery. The battery performance of as-prepared $MoSe_2$ nanosheets is studied in the two-electrode configuration in an alkaline medium.

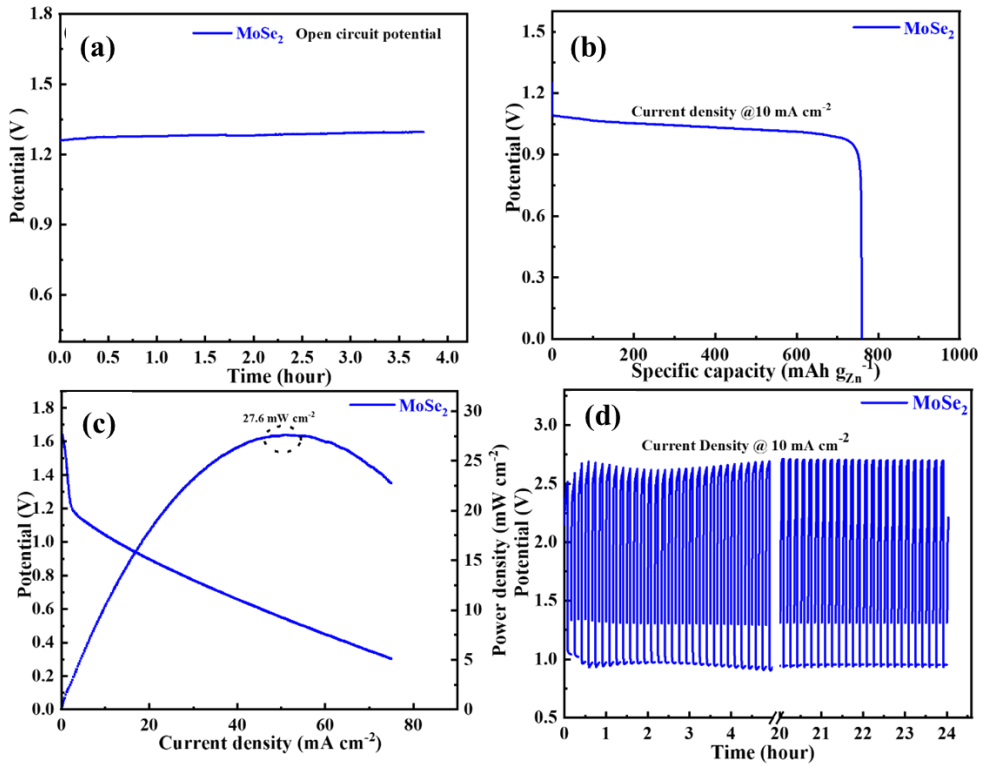

Figure 6.3 *(a) OCP curve, (b) Specific capacity curve at current density of 10 mA cm^{-2}, (c) discharge voltage curve and corresponding power density plot and (d) charging-discharging curves at a current density of 10 mA cm^{-2} for fabricated zinc-air battery using $MoSe_2$ nanosheets.*

The OCP of the assembled battery cell is found ~1.28 V, with high degree of stability tested for around 4 h, as shown in **Figure 6.3(a)**. Further discharge capacity of fabricated device is studied at discharge current density of 10 mA cm^{-2}, as shown in **Figure 6.3(b)**. Based on the mass consumption of Zn anode, we have achieved high specific capacity of 760 mAh g^{-1} using **equation 6.14** for fabricated zinc-air battery. The discharge polarization

curves of the batteries are shown in **Figure 6.3(c)**. The energy density is calculated by obtaining the integrated area of potential *vs.* specific capacity curve (Figure 6b). The energy density of fabricated zinc-air batteries can be obtained from the **equation 6.15.** Energy density of around 783 Wh kg^{-1}, is found for $MoSe_2$-based zinc-air battery. The maximum power density of fabricated zinc-air battery is found to be 27.5 mW cm^{-2} at current density of 51 mA cm^{-2} using **equation 6.16** exhibiting excellent power delivering capacity. Further rechargeability of the fabricated device has also been investigated. The rechargeable stability of fabricated zinc-air is shown in **Figure 6.3(d)**. It shows high degree of stability for continuous 24 hours exhibiting constant discharge potential. We have confirmed the phase of the $MoSe_2$ nanosheets of the air cathode before and after the battery's cyclic stability test *via*. Raman spectroscopy, as shown in **Figure 6.4**. It clearly indicates the phases of the $MoSe_2$ remain stable during battery operation.

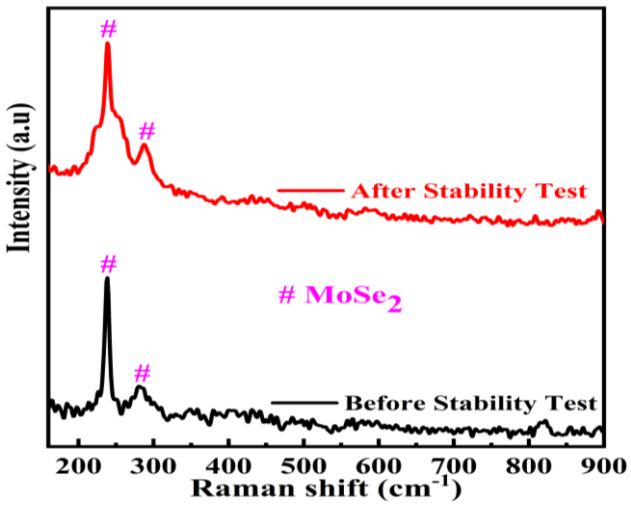

Figure 6.4 *Raman spectra for $MoSe_2$ nanosheets-based air cathode before and after cyclic durability of battery stability.*

6.2.3 Zinc-air battery performance using $NiCo_2O_4$/NiO-$MoSe_2$ hybrid nanostructure as air cathode

The hydrothermally produced $NiCo_2O_4$/NiO-$MoSe_2$ hybrid nanostructure shows good catalytic activity for OER (as discussed in chapter 4), that prompted us to use them as an air

cathode in zinc-air battery. The battery performance of as-prepared $NiCo_2O_4$/NiO and $NiCo_2O_4$/NiO-$MoSe_2$-$MoSe_2$ hybrid nanostructure is performed in the two-electrode configuration in an alkaline medium. The OCP, specific capacity, energy density, and power density of designed batteries have been calculated to understand their performance. The OCP for prepared battery cells are observed nearly constant for longer durations, as shown in **Figure 6.5(a)**. We observe that $NiCo_2O_4$/NiO-$MoSe_2$ hybrid nanostructure-based zinc-air battery shows the high OCP of 1.42 V compared to 1.2 V for pristine $NiCo_2O_4$/NiO cathodes-based battery. The specific capacities of zinc-air batteries with different cathode materials are calculated using the following **equation 6.14**. The weight of the consumed zinc electrode is used to normalize the calculation of specific capacity. The complete discharge curves for prepared batteries at current density of 10 mA cm^{-2} are shown in **Figure 6.5(b)**. The $NiCo_2O_4$/NiO, and $NiCo_2O_4$/NiO-$MoSe_2$ hybrid nanostructure cathodes-based zinc-air batteries show specific capacities of 788, and 1023 mA h g_{Zn}^{-1}, respectively. The $NiCo_2O_4$/NiO-$MoSe_2$ hybrid nanostructure-based zinc-air battery shows better specific capacity compared to pristine $NiCo_2O_4$/NiO due to excellent electrocatalytic activity (lower Tafel slope and overpotential) resulting from the synergistic effect between $MoSe_2$ and $NiCo_2O_4$/NiO. The energy density of fabricated zinc-air batteries can be obtained from the **equation 6.15**. The energy densities can be calculated by obtaining the integrated area of potential vs specific capacity curve. Energy densities of around 795, and 1195 W h kg^{-1} are found for $NiCo_2O_4$/NiO, and $NiCo_2O_4$/NiO-$MoSe_2$ hybrid nanostructure-based zinc-air batteries, respectively, again suggesting the better performance of hybrid nanostructure-based zinc-air battery.

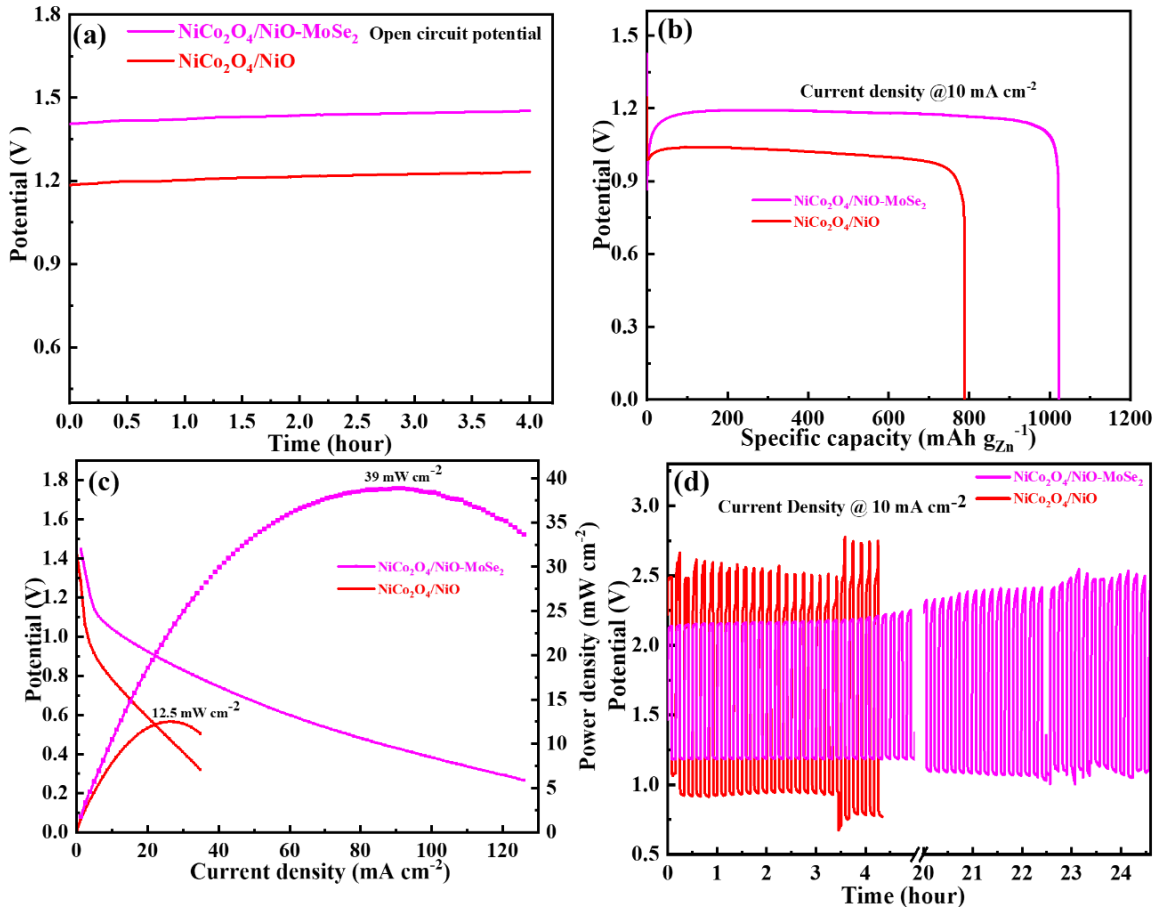

Figure 6.5 *(a) OCP curve, (b) Specific capacity curve at current density of 10 mA cm^{-2}, (c) discharge voltage curves and corresponding power density plots and (d) charging-discharging curves at a current density of 10 mA cm^{-2} for fabricated zinc-air batteries.*

Figure 6.5 (c) shows the discharge polarization curves for prepared batteries, indicating a maximum power density of 39 mW cm^{-2} for $NiCo_2O_4$/NiO-$MoSe_2$ hybrid nanostructure-based battery at a current density of 89.4 mA cm^{-2} compared to the power density of 12.5 mW cm^{-2} at current density of 27.6 mA cm^{-2} for $NiCo_2O_4$/NiO based battery. Further, the rechargeable capability and stability of prepared zinc-air batteries are tested with 5 minutes of charging and discharging cycles, each at the current density of 10 mA cm^{-2}, as shown in **Figure 6.5 (d)**. The $NiCo_2O_4$/NiO-$MoSe_2$ hybrid nanostructure-based battery shows remarkable stability for around 24 h compared to around 4 h for pristine $NiCo_2O_4$/NiO based batteries. The excellent stability of $MoSe_2$ enhances the stability of the hybrid nanostructure and makes it suitable for durable high-performance zinc-air battery. We have confirmed the phase of the

$NiCo_2O_4$/NiO-$MoSe_2$ hybrid nanostructure of the air cathode before and after the battery's cyclic stability test via Raman spectroscopy, as shown in **Figure 6.6**. It clearly indicates the phases of the $NiCo_2O_4$/NiO-$MoSe_2$ hybrid nanostructure remain stable during battery operation.

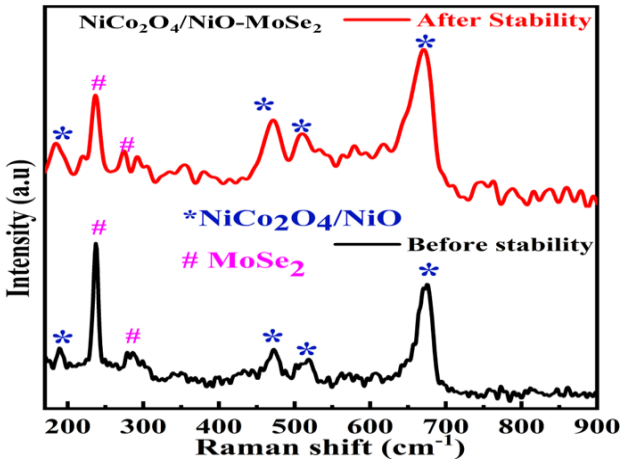

Figure 6.6 *Raman spectra for $NiCo_2O_4$/NiO-$MoSe_2$ hybrid nanostructure-based air cathode before and after cyclic durability of battery stability.*

6.2.4 Zinc-air battery performance using $CoFe_2O_4$-$MoSe_2$ hybrid nanostructure as air cathode

The hydrothermally prepared $CoFe_2O_4$-$MoSe_2$ hybrid nanostructure shows good catalytic activity for OER (as discussed in chapter 4), which prompted us to use it as an air cathode in zinc-air battery. The battery performance of as-prepared pristine $CoFe_2O_4$ and $CoFe_2O_4$-$MoSe_2$ hybrid nanostructures in an alkaline medium is performed in the two-electrode configuration. **Figure 6.7 (a)** shows that the $CoFe_2O_4$-$MoSe_2$ hybrid nanostructure-based zinc-air battery has a higher OCP of 1.34 V as compared to $CoFe_2O_4$ (1.21 V). Further, zinc-air batteries designed with these cathode materials have been discharged at the constant current density of 10 mA.cm^{-2} and specific capacities of the same are calculated using the following **equation 6.14.** The designed $CoFe_2O_4$-$MoSe_2$, and $CoFe_2O_4$ based zinc-air batteries show specific capacities of 888 and 570 mA h g_{Zn}^{-1}, respectively. The higher specific capacity of $CoFe_2O_4$-$MoSe_2$ hybrid nanostructure compared to pristine $CoFe_2O_4$ is due to its higher

electrocatalytic activity compared to pristine $CoFe_2O_4$, due to synergistic effect of $MoSe_2$ and $CoFe_2O_4$. Further, the energy densities of the designed batteries have been evaluated using the **equation 6.14**.

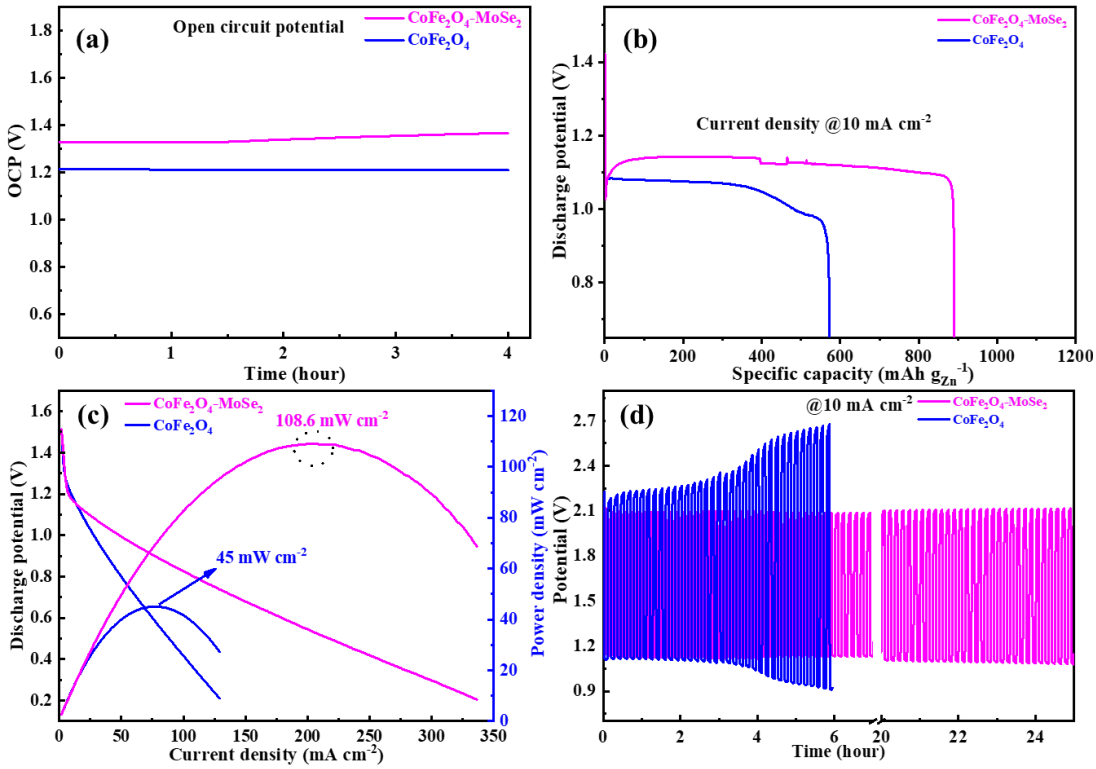

Figure 6.7 *(a) Open circuit potentials, (b) constant discharge curves at 10 mA cm^{-2}, (c) galvanodynamic discharge and power density curves, (d) cyclic stability curves of 5 min charge and 5 min discharge at 10 mA cm^{-2} of $CoFe_2O_4$ and $CoFe_2O_4$-$MoSe_2$ hybrid nanostructure based zinc-air batteries.*

The energy density of the designed battery is equal to the area of potential vs. specific capacity curve (**Figure 6.7(b)**) and obtained energy densities are found to be 998 and 601 W h kg^{-1} for $CoFe_2O_4$-$MoSe_2$ hybrid nanostructure and pristine $CoFe_2O_4$ based zinc-air batteries, respectively, again suggesting the better performance of $CoFe_2O_4$-$MoSe_2$ hybrid nanostructure-based zinc-air battery. **Figure 6.7(c)** shows the discharge polarization profiles for the designed batteries, highlighting the $CoFe_2O_4$-$MoSe_2$ hybrid nanostructure-based zinc-air battery with higher power density of ~108.6 mW cm^{-2} at a discharge current density of 213.5 mA cm^{-2} in comparison to $CoFe_2O_4$ based zinc-air batteries (power density~45 mW.cm^{-2} at a current

density of 80.6 mA.cm^{-2}). Furthermore, the rechargeable capability and stability of the prepared zinc-air batteries are evaluated by performing 5 minutes of charging and discharging cycles, each conducted at a current density of 10 mA cm^{-2}, as depicted in **Figure 6.7(d)**. The $CoFe_2O_4$-$MoSe_2$ hybrid nanostructures-based zinc-air batteries exhibit higher stability over approximately 24 hours and exhibit higher discharge potential than pristine $CoFe_2O_4$-based zinc-air batteries (~ 6 hours). We have confirmed the phase of the $CoFe_2O_4$-$MoSe_2$ hybrid nanostructure of the air cathode before and after the battery's cyclic stability test via Raman spectroscopy, as shown in **Figure 6.8**. It clearly indicates the phase of $CoFe_2O_4$-$MoSe_2$ hybrid nanostructure remain stable during battery operation.

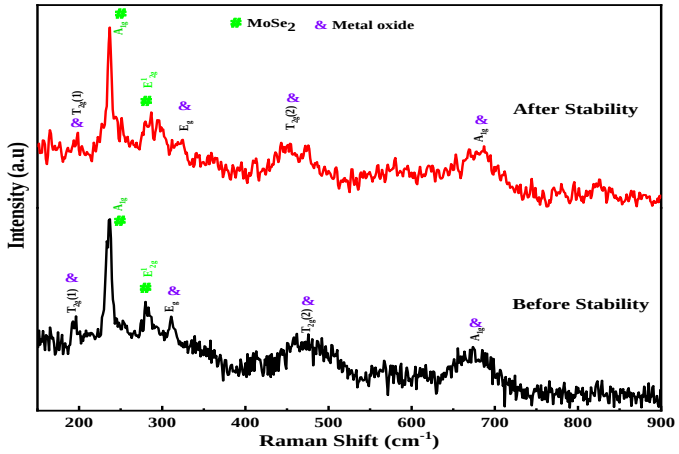

Figure 6.8 *Raman spectra for $CoFe_2O_4$-$MoSe_2$ hybrid nanostructure-based air cathode before and after cyclic durability of battery stability.*

6.2.5 Zinc-air battery performance using $NiFe_2O_4$-$MoSe_2$ hybrid nanostructure as air cathode

The hydrothermally prepared $NiFe_2O_4$-$MoSe_2$ hybrid nanostructure shows the highest catalytic activity for OER (as discussed in chapter 4), which prompted us to use it as an air cathode in zinc-air battery. The battery performance of as-prepared $NiFe_2O_4$ and $NiFe_2O_4$-$MoSe_2$ hybrid nanostructures as air cathode in an alkaline medium (6M KOH+0.2M zinc acetate) is performed in the two-electrode configuration. **Figure 6.9 (a)** shows that the $NiFe_2O_4$-$MoSe_2$ hybrid nanostructure-based zinc-air battery has a higher OCP of 1.43 V as

compared to pristine $NiFe_2O_4$ based zinc-air battery (1.26 V). Further, zinc-air batteries designed with different cathode materials have been discharged at the constant current density of 10 mA cm^{-2} and specific capacities of the same are calculated using the **equation 6.14**. **Figure 6.9 (b)** illustrate that the designed $NiFe_2O_4$-$MoSe_2$ hybrid and pristine $NiFe_2O_4$-based zinc-air batteries show specific capacities of 1025 and 656 mA h g_{Zn}^{-1}, respectively. The higher specific capacity of $NiFe_2O_4$-$MoSe_2$ hybrid nanostructure compared to pristine $NiFe_2O_4$ is due to its higher electrocatalytic activity and the synergistic effect between $MoSe_2$ and $NiFe_2O_4$ in hybrid nanostructure. Further, the energy density of the designed batteries has been evaluated using the **equation 6.15.** The energy density of the designed battery is equal to the area of potential vs. specific capacity curve and obtained energy densities are found to be 1204 and 714 W h kg^{-1} for $NiFe_2O_4$-$MoSe_2$ hybrid and pristine $NiFe_2O_4$ based zinc-air batteries, respectively, again suggesting the better performance of $NiFe_2O_4$-$MoSe_2$ hybrid nanostructure-based zinc-air battery.

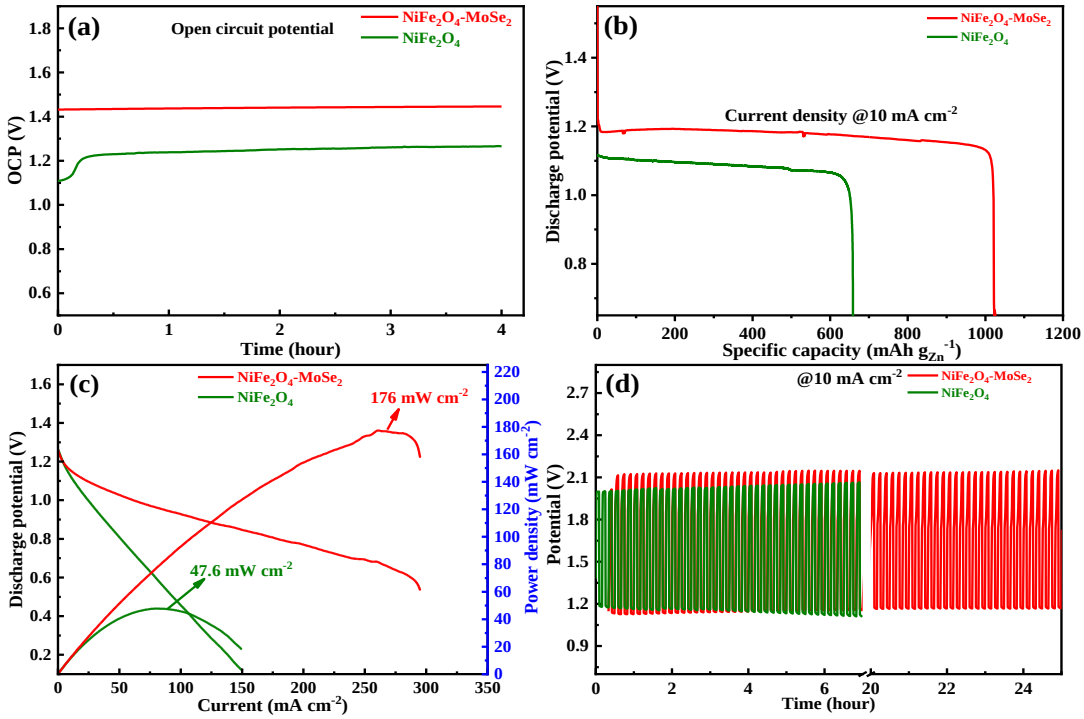

Figure 6.9 *(a) Open circuit potentials, (b) constant discharge curves at 10 mA cm^{-2}, (c) galvanodynamic discharge and power density curves, (d) cyclic stability curves of 5 min charge and 5 min discharge at 10 mA cm^{-2} of $NiFe_2O_4$ and $NiFe_2O_4$-$MoSe_2$ hybrid nanostructure based zinc-air batteries.*

Figure 6.9(c) shows the discharge polarization profiles for the designed batteries, highlighting the $NiFe_2O_4$-$MoSe_2$ hybrid nanostructure-based zinc-air battery with the maximum power density of 176 mW cm^{-2} at a discharge current density of 269 mA cm^{-2} in comparison to pristine $NiFe_2O_4$ based zinc-air batteries (power density ~ 47.6 mW cm^{-2} at a current density of 81.5 mA cm^{-2}). Furthermore, the rechargeable capability and stability of the prepared zinc-air batteries are evaluated by performing 5 minutes of charging and discharging cycles each, conducted at a current density of 10 mA cm^{-2}, as depicted in **Figure 6.9(d)**. Impressively, the $NiFe_2O_4$-$MoSe_2$ hybrid nanostructures-based zinc-air battery shows exceptional stability over approximately 24 hours and exhibits higher discharge potential than $NiFe_2O_4$ based zinc-air battery. We have confirmed the phase of the $NiFe_2O_4$-$MoSe_2$ hybrid nanostructure of the air cathode before and after the battery's cyclic stability test via Raman spectroscopy, as shown in **Figure 6.10**. It clearly indicates that $MoSe_2$ and $NiFe_2O_4$ in $NiFe_2O_4$-$MoSe_2$ hybrid nanostructure remain stable during battery operation.

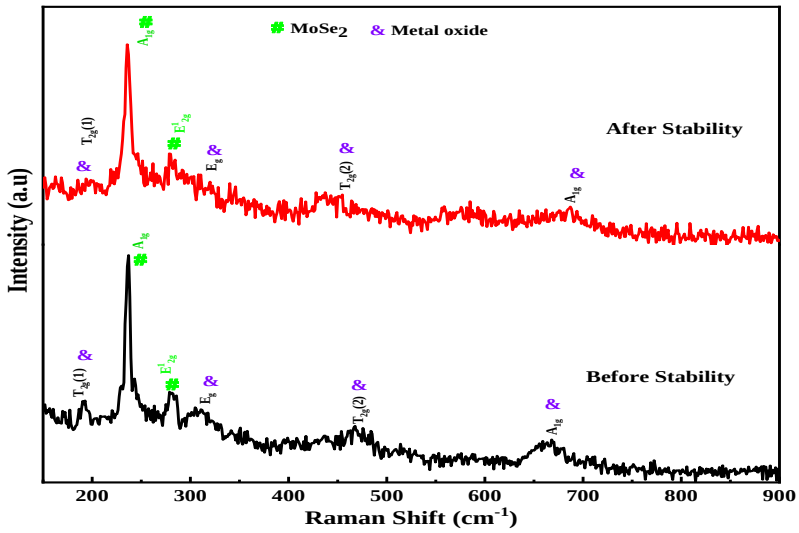

Figure 6.10 *Raman spectra for $NiFe_2O_4$-$MoSe_2$ hybrid nanostructure-based air cathode before and after cyclic durability of battery stability.*

Battery performance of our hybrid nanostructures based zinc-air batteries are found better than others reported literatures, as summarized in **Table 6.1.** This could be due to the synergistic effect between $MoSe_2$ and bimetal oxides ($NiCo_2O_4$/NiO, $CoFe_2O_4$ and $NiFe_2O_4$)

in their respective hybrid nanostructures. The synergy between $MoSe_2$ and bimetal oxide may lead to higher number of active sites and less charge transfer resistance, which may lead to better battery performance.

Table 6.1 The comparative performance summary of rechargeable zinc-air batteries with other literature reports.

Materials	**Electrolyte**	**OCP (V)**	**Specific capacity (mA h g_{Zn}^{-1}) @10 mA cm^{-2}**	**Energy density (W h Kg_{Zn}^{-1})**	**Ref.**
$MoSe_2$	6M KOH + 0.2 M $Zn(CH_3COO)_2$	1.25	760	783	Thesis work
$CoFe_2O_4$	6M KOH + 0.2 M $Zn(CH_3COO)_2$	1.21	570	601	Thesis work
$NiCo_2O_4$/NiO	6M KOH + 0.2 M $Zn(CH_3COO)_2$	1.2	788	795	Thesis work
$NiFe_2O_4$	6M KOH + 0.2 M $Zn(CH_3COO)_2$	1.26	656	714	Thesis work
$CoFe_2O_4$-$MoSe_2$ hybrid nanostructure	6M KOH + 0.2 M $Zn(CH_3COO)_2$	1.34	888	998	Thesis work
$NiCo_2O_4$/NiO-$MoSe_2$ hybrid	6M KOH + 0.2 M $Zn(CH_3COO)_2$	1.42	1023	1195	Thesis work
$NiFe_2O_4$-$MoSe_2$ hybrid nanostructure	6M KOH + 0.2 M $Zn(CH_3COO)_2$	1.43	1025	1204	Thesis work
NiO/$NiCo_2O_4$ porous nanofiber	6M KOH + 0.2 M $Zn(CH_3COO)_2$	1.47	814	911	[195]
$NiCo_2O_4$@FeNi LDH	6M KOH + 0.2 M $Zn(CH_3COO)_2$	1.40	810	--	[196]
N-doped NiO	6M KOH	1.44	819	--	[197]
NiO/CoN	6M KOH	1.46	648	836	[198]
CoFe/$CoFe_2O_4$@NC	6M KOH + 0.2 M $Zn(CH_3COO)_2$	1.53	774.8	905	[199]
$NiCo_2O_4$/N-G	6M KOH + 0.2 M $Zn(CH_3COO)_2$	--	792.6	879	[200]
O-$Co_{1-x}Mo_xSe_2$	PVA-KOH	1.4	723	783	[201]
FePc||$NiFe_2O_4$/G	PVA-KOH+ $Zn(CH_3COO)_2$	1.39	741	--	[154]

6.3 Conclusion

This chapter presents the electrochemical response of $MoSe_2$ and its hybrid nanostructures with $CoFe_2O_4$, $NiCo_2O_4$/NiO, and $NiFe_2O_4$ as air cathodes for zinc-air batteries. The open-circuit voltage, specific capacity, energy density, power density, and rechargeability of the zinc-air batteries have been measured and analyzed. The results reveal that the hybrid nanostructures-based zinc-air batteries exhibit higher performance than the pristine $MoSe_2$ and pristine metal oxides-based zinc-air batteries due to the improved OER activity and reduced charge transfer resistance in hybrid nanostructures. Among all examined zinc-air batteries in the present work, $NiFe_2O_4$-$MoSe_2$ based zinc-air battery shows the best performance, with an open-circuit voltage of 1.43 V, a specific capacity of 1025 mA h g_{Zn}^{-1}, an energy density of 1204 W h kg_{Zn}^{-1}, and a high-power density of 176 mW cm^{-2}. The $NiFe_2O_4$-$MoSe_2$-based zinc-air battery also demonstrates excellent stability and durability for 24 hours of continuous charge-discharge cycles.